Hindawi
International Journal of Antennas and Propagation
Volume 2019, Article ID 4512532, 12 pages
https://doi.org/10.1155/2019/4512532

Research Article

Design of a Dual-Band Frequency Reconfigurable Patch Antenna Based on Characteristic Modes

Zakaria Mahlaoui,[1,2] **Eva Antonino-Daviu**,[1] **Adnane Latif**,[2] **and Miguel Ferrando-Bataller**[1]

[1]*Instituto de Telecomunicaciones y Aplicaciones Multimedia, Universitat Politècnica de València, 46022, Spain*
[2]*Information Technology and Modeling Laboratory, National School of Applied Sciences, Cadi Ayyad University, 40000, Morocco*

Correspondence should be addressed to Zakaria Mahlaoui; mahza@doctor.upv.es

Received 30 November 2018; Accepted 4 February 2019; Published 31 March 2019

Academic Editor: Yuan Yao

A frequency reconfigurable patch antenna design based on the characteristic mode analysis is presented. The antenna presents a reconfigurable lower band and a steady band at higher frequencies. A slot is etched on the ground plane of the antenna, where two varactor diodes are placed on each side of the slot in order to tune the lower band. The first resonant frequency shifts down by varying the reverse voltage of the varactor, whereas the second operating frequency keeps stable. The proposed antenna is designed to cover WLAN bands, offering a first band operating at 2 GHz and a second band ranging from 5.3 GHz to 5.8 GHz. A prototype has been fabricated and measurements are provided, which validate the proposed analysis, method, and design procedure.

1. Introduction

In a wireless system, the antenna is a decisive component. A simple and appropriate design can fulfil the system requirements and improve the global system performance. Patch antennas are one of the simplest antenna structures, and they have been widely used over the years due to their characteristics of low cost, lightweight, low profile, and ease of integration.

Nevertheless, interference to the communication systems can exist because of the presence of different wireless applications who are using the same frequency band. As an example, in the Industrial, Scientific, and Medical (ISM) radio bands and the Unlicensed National Information Infrastructure (referred to as U-NII) bands used by IEEE 802.11 devices, the use of those bands is sometimes excessive by the Wi-Fi customers and leads to the presence of interferences because the access to this radio spectrum is without the need of restrictions and regulations that might be applicable elsewhere.

In addition, this unlicensed band operates over many frequencies, and from an antenna design perspective, UWB antenna with a band suppression feature can be one solution [1], but the cost and the difficulty here are increased. To overcome this issue, frequency reconfigurable antennas are proposed, where a dynamic modification of the operating frequency of the antenna brings flexibility to the communication system. This kind of antenna will not cover all the frequency bands simultaneously but provides several dynamically selectable narrow frequency bands and, within these bands, exhibits higher flexibility than that achievable with conventional wide-band and multiple band antenna solutions [2, 3]. Reconfigurability can be achieved by using electronic components to tune antenna characteristics such as PIN diodes [4–6], varactors [7, 8], and MEMS switches [9, 10] or changing material properties [11].

Hence, this paper presents an antenna with two bands suitable for WLAN applications. Work done in [3] proposed a similar simulation approach but only at 5 GHz band. However, the antenna proposed here operates at 2 GHz band, which will be a reconfigurable band, and at a second one that ranges from 5.3 GHz to 5.8 GHz, which is a steady band. A Defected Ground Structure (DGS) [12] consisting in a rectangular shape slot embedded in the ground plane is

proposed and has been studied using characteristic mode analysis (CMA), which provides interesting physical insight into the antenna behavior [13]. Varactor diodes are used to perform the selectivity over the frequency band. In this part, two simulation approaches are followed: the ideal case and the equivalent circuit case. At the end, a prototype has been fabricated and measurements have been made to validate the simulation results.

2. Characteristic Mode Analysis

2.1. Brief Introduction to the Theory of Characteristic Modes. Characteristic mode analysis (CMA) provides understanding into the physical phenomena associated to the radiating behavior of an antenna with arbitrary shape. Therefore, it helps to simplify the analysis, synthesis, and optimization of antennas [13]. By solving a generalized eigenvalue problem shown in equation 1, involving the impedance matrix of the Method of Moments (MoM), a set of orthogonal eigencurrents together with their associated eigenvalues are obtained. Due to the orthogonality of the eigencurrents, the total current on the surface of the conductor can be expanded into those modes. The eigenvalues provide information about the radiating behavior of the associated mode. Also, the quantities characteristic angle α_n in equation 2 and modal significance MS_n in equation 3 can be calculated, which are associated to the eigenvalue λ_n in equation 1.

As defined in [14], the following generalized eigenvalue equation is expressed by

$$X(J_n) = \lambda_n R(J_n), \tag{1}$$

where λ_n are the eigenfunctions, J_n are the eigencurrents, and R and X are, respectively, the real and imaginary parts of the impedance matrix of the MoM.

The characteristic angle provides a way to better show the mode behavior near resonance, and it is defined as

$$\alpha_n = 180^\circ - \tan^{-1}(\lambda_n). \tag{2}$$

The modal significance (MS_n) measures the contribution of each mode in the total electromagnetic response to a given source. It is described by

$$\mathrm{MS}_n = \left| \frac{1}{1 + j\lambda_n} \right|. \tag{3}$$

2.2. Characteristic Mode Analysis of a Patch Antenna over a Finite Ground Plane. Let us perform the characteristic mode analysis (CMA) of a metallic rectangular plate of 29 mm × 31 mm over a rectangular ground plane of 35 mm × 50 mm. Figure 1 shows the geometry of the structure to analyze, where the separation between the two plates is $h = 1.524$ mm. No substrate is used.

The characteristic angle α_n associated to the first six CM of the structure is shown in Figure 2. Current distribution corresponding to these six modes at its resonance frequency ($\alpha_n = 180^\circ$) is plotted in Figure 3, where arrows have been included for the sake of understanding to indicate the direction of the current in the ground plane and dashed lines represent nulls of current. As can be observed, each mode presents a specific current distribution, with vertical and/or horizontal currents.

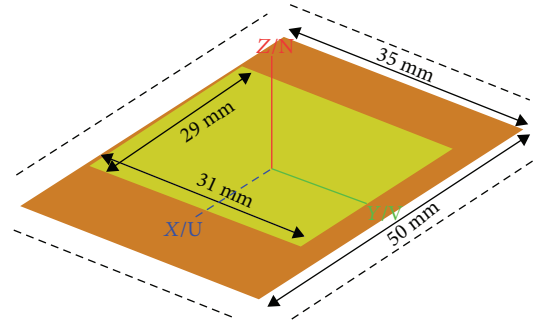

Figure 1: Patch antenna over a finite rectangular ground plane to analyze with CMA. Separation between the two plates is 1.524 mm.

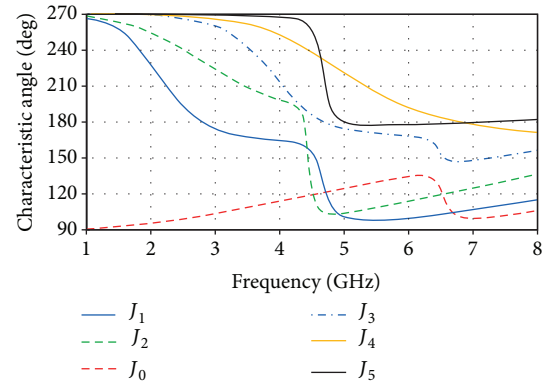

Figure 2: Characteristic angle associated to the first six CM of the patch antenna shown in Figure 1.

CM are intrinsic to any structure but their excitation depends on the feeding mechanism used. If the patch antenna is excited at its longer edge by a microstrip line, modes with current distributed along the x-axis and with opposite flow direction in the patch and in the ground plane will be excited. Therefore, according to Figure 3, modes J_1 and J_4 are the ones that will be excited. As each mode resonates at a different frequency ($\alpha_n = 180^\circ$), two operating bands will be achieved, obtaining a dual-band antenna.

Now, in order to create a tunable band for the first operating band, a narrow rectangular slot with two tunable capacitors should be inserted in the antenna at the appropriate place, so as to not disturb the second operating band that should be fixed. Looking at the current distribution associated to modes J_1 and J_4, we can see that the slot should be inserted in the center of the ground plane. Remark that the unidirectional radiation behavior of the patch is lost when the slot is etched in the ground plane, as back radiation will appear in this case. For applications where bidirectional radiation is needed, the proposed antenna with defected ground plane (slotted ground plane) can be used.

Figure 4 depicts the geometry of the proposed defected ground plane of the patch antenna. As a null of current is present at the position of the slot for mode J_4, this mode will

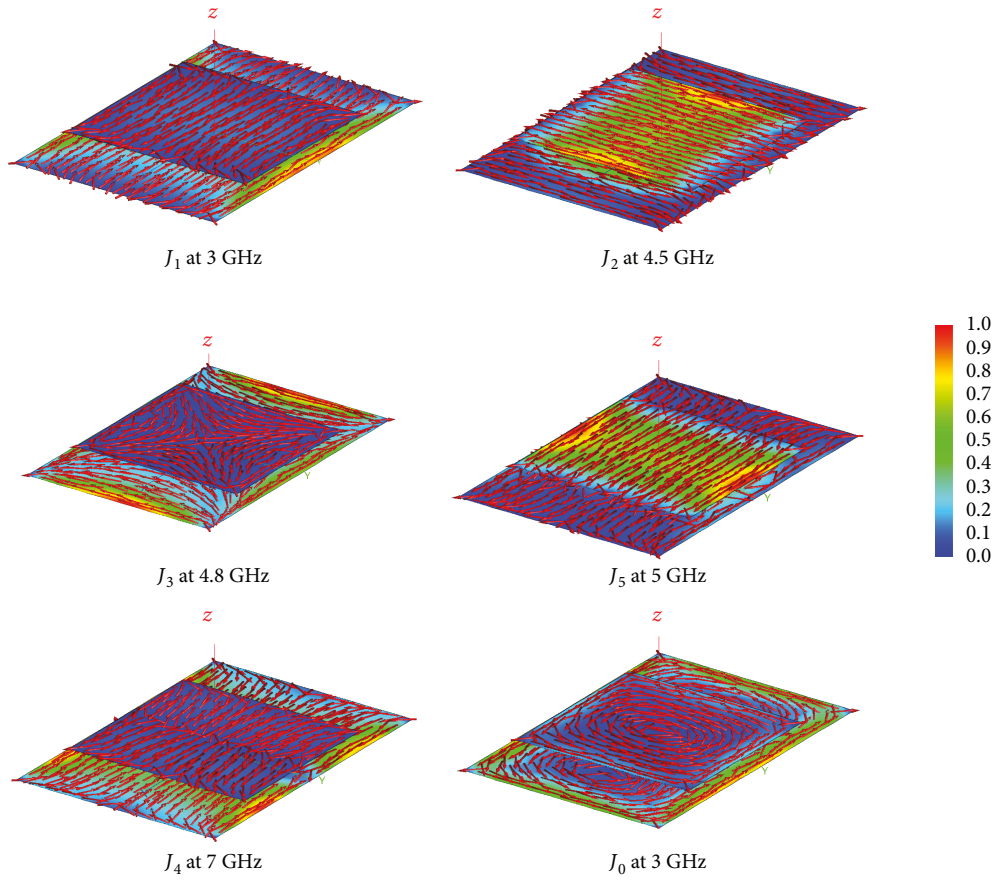

Figure 3: Current distribution of the first six CM of a patch antenna over a rectangular ground plane, near the resonance frequency. Arrows indicate the direction of the current in the ground plane and dashed lines indicate nulls of current.

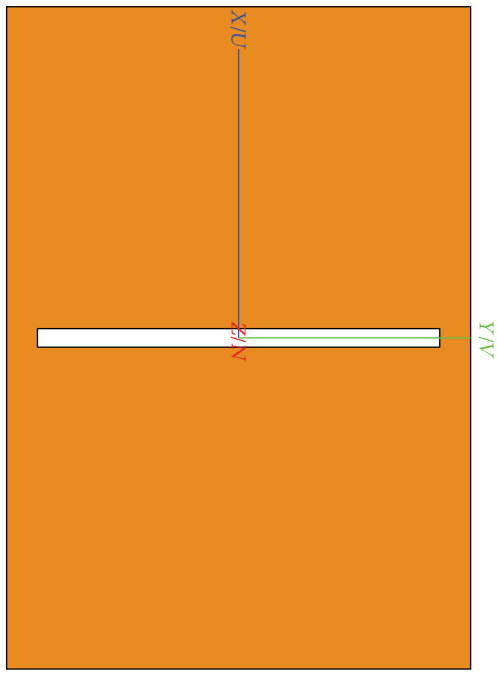

Figure 4: Defected ground plane (DGP) for the reconfigurable dual-band antenna.

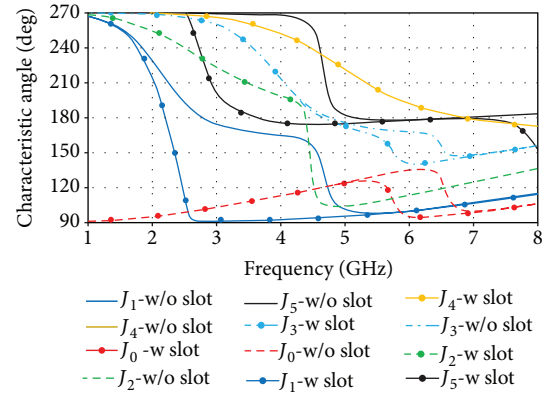

Figure 5: Comparison of the characteristic angle associated to the first six CM of the patch antenna over a ground plane with and without slot.

not be affected by the presence of the slot, while mode J_1 will be. This fact can be observed in Figure 5, where a comparison of the characteristic angle of the original structure and the structure including the slot is shown. As it can be seen, the resonant frequency of mode J_1 is shifted down due to the presence of the slot, while mode J_4 is not perturbed.

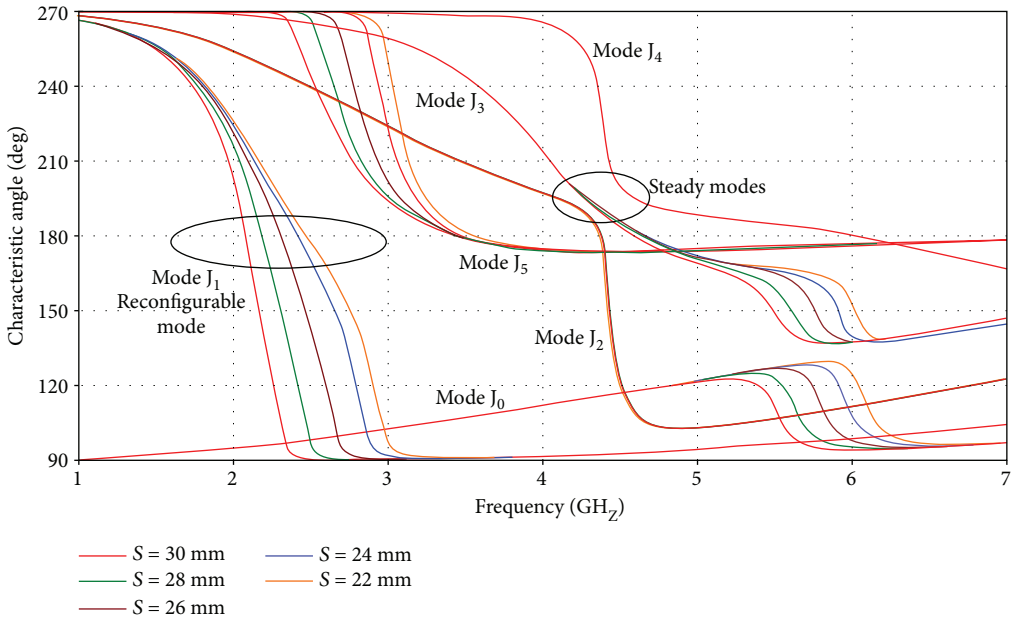

Figure 6: Characteristic angle variation with the slot length (S) for the first six CM over frequency.

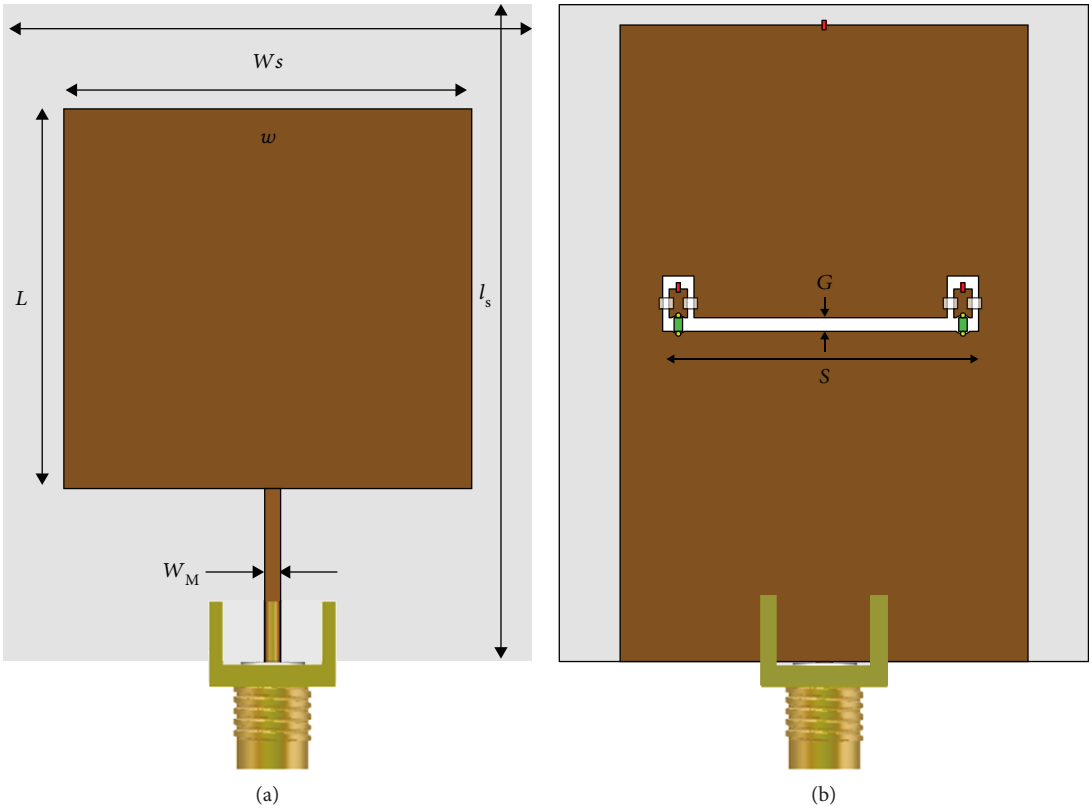

Figure 7: Antenna geometry. (a) Front view. (b) Back view.

Moreover, Figure 6 shows the characteristic angle of the first six modes when varying the slot length (S). As seen, the variation of the slot length affects modes J_1 and J_5, modifying their characteristic angle. Modes J_0, J_2, J_3, and J_4

Table 1: Dimension of the designed antenna.

Parameter	W	L	Ws	Ls	W_M	G	S	h
Value (mm)	31	29	35	50	1.25	1	30	1.524

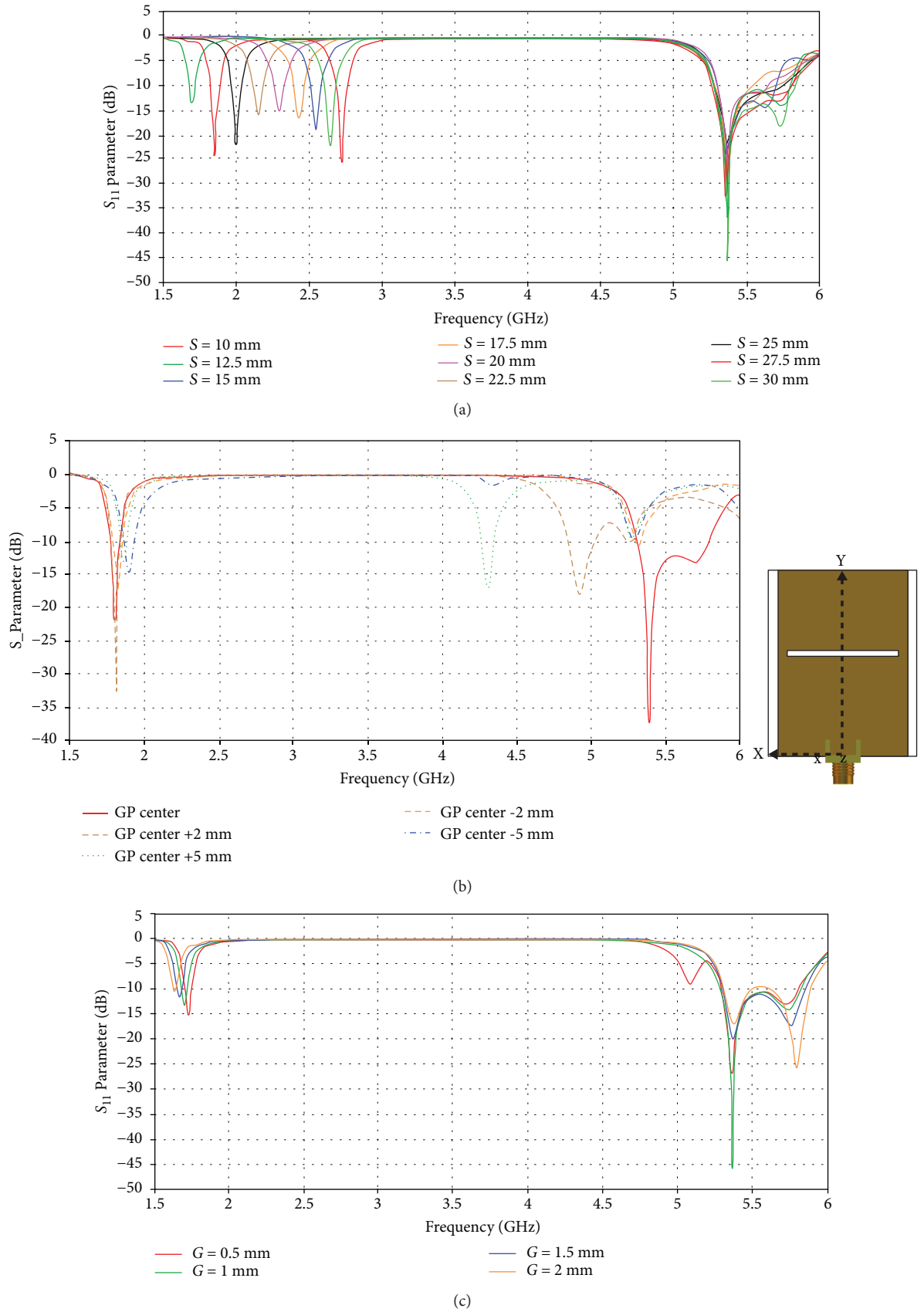

FIGURE 8: S_{11} parameter variation with (a) the slot length (S), (b) the slot position along the y-axis (*GP center*), (c) the slot width (g).

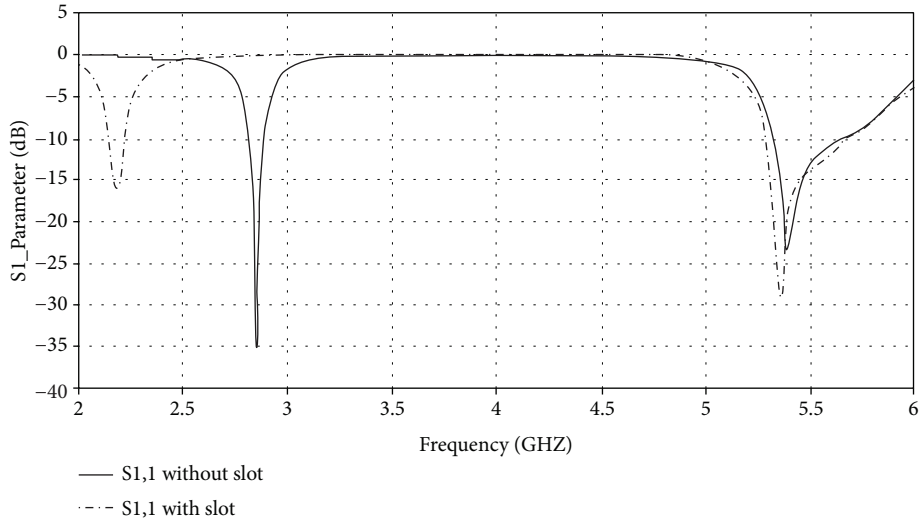

Figure 9: S_{11} parameter of the antenna without slot and with slot.

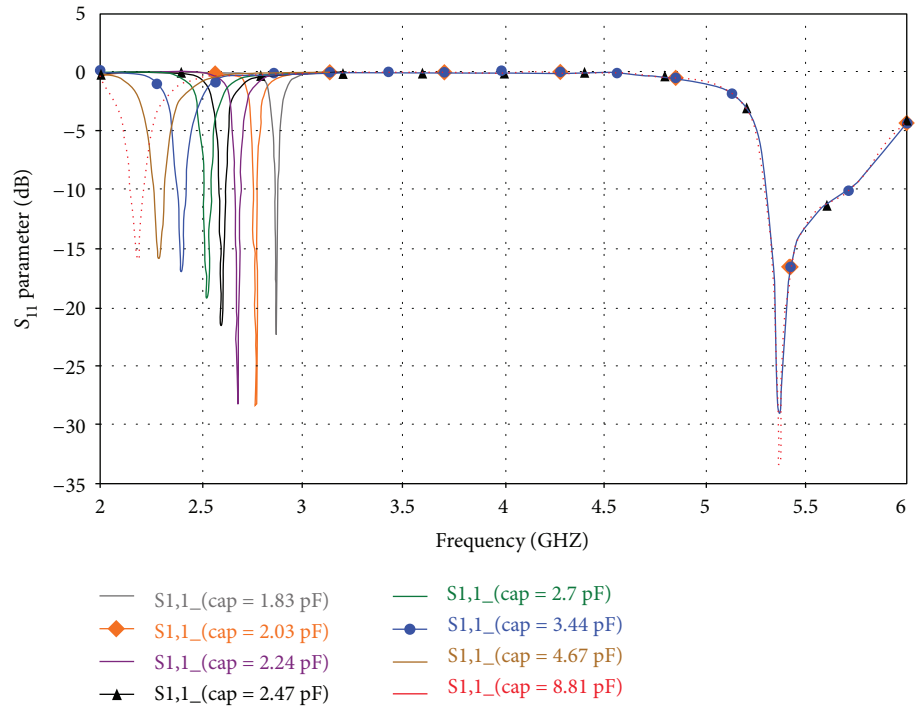

Figure 10: S_{11} parameter of the ideal case using capacitors.

are showing a constant behavior as they are conserving the same characteristic angle and resonant frequency even though the slot length is changing.

As modes J_1 and J_4 are excited in the proposed antenna, if the slot is loaded with variable capacitors, the resonance frequency of mode J_1 can be tuned, keeping the resonance frequency of mode J_4 steady. This will be shown in the next section.

3. Antenna Description and Simulations

3.1. Antenna Geometry. Figure 7 shows the geometry of the proposed reconfigurable dual-band antenna. As observed, the antenna consists of a rectangular patch with length L and width W, where entire dimensions of the ground plane are $Ls \times Ws$. The substrate used is Rogers RO3003, which is a lossy substrate with a dielectric constant of $\varepsilon_r = 3$ and loss tangent $\tan\delta = 0.001$. The patch antenna is fed at the longer edge by a microstrip line of width W_M connected to a coaxial SMA port of 50 Ω. As the objective is to obtain two bands (lower band at 2 GHz and upper band centered at 5 GHz), a slot of length S and width G is etched in the ground plane as described in the previous section. Each side of the slot is loaded with a varactor diode, to keep the symmetry. The model of the varactor adopted in this work is the SMV2025

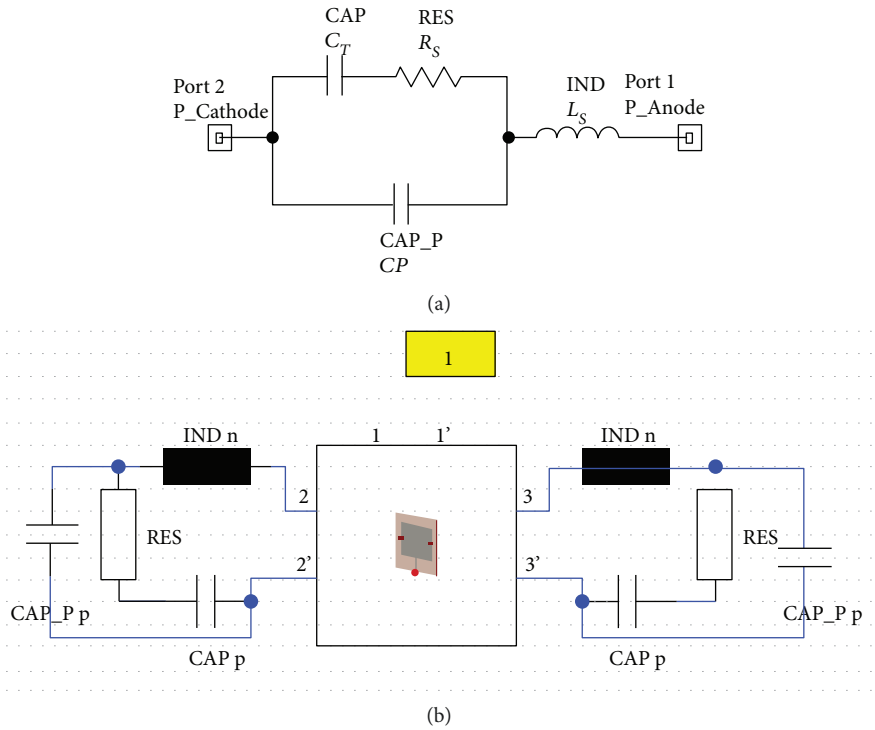

Figure 11: (a) Equivalent circuit of the diode varactor. (b) Schematic design of the antenna.

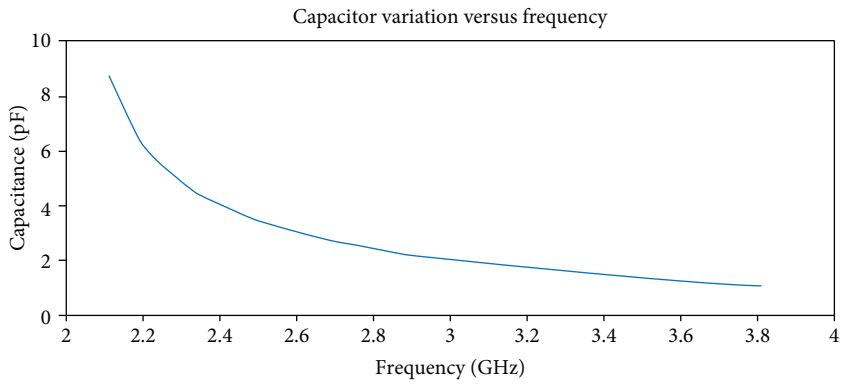

Figure 12: Variation of the varactor capacitance over frequency [15].

surface mount, hyperabrupt tuning varactor diode [15]. The simulation design is performed by using CST software, based on the simplified theoretical formulations that have been described in [16]. The final dimensions are shown in Table 1.

3.2. Simulation Results

3.2.1. Parametric Study of the Slot. In Figure 6, it has been presented the characteristic angle variation of the modes when varying the slot length (S), showing a variation in the resonance frequency of mode J_1 (mode of the tunable band). In Figure 8(a), the S_{11} parameter for different slot lengths is shown. As it can be observed, the slot length affects the first frequency band (reconfigurable band).

In order to obtain good results, the slot should be inserted in the center of the ground plane. Figure 8(b) shows the S_{11} parameter for different slot positions on the y-axis, with respect to the center of the ground plane (i.e., GP center is the distance from the center of the ground plane along the y-axis).

Finally, Figure 8(c) presents the S_{11} parameter for different slot widths. As observed, the slot width affects the matching of the frequency bands.

3.2.2. Reconfigurable Antenna Simulation Methods. Figure 9 shows the return losses of the antenna without slot and with slot. As shown by the CMA and as can be observed in Figure 9, the effect of adding a slot in the ground plane of the antenna shifts down the lower band, from 2.8 GHz to 2.2 GHz. It should be mentioned that the band achieved by the slot could be obtained by using the length of 0.165λ. Likewise, the second frequency band holds in a steady regime without any disturbance coming from the slot, as seen before.

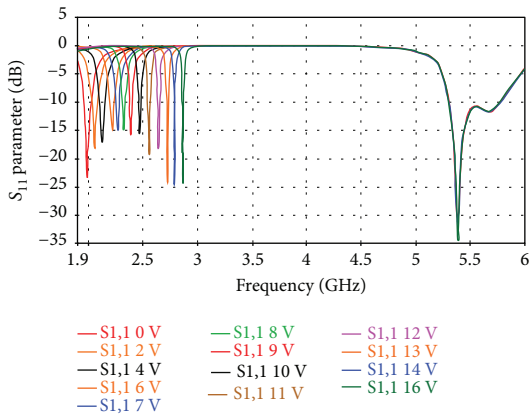

FIGURE 13: S_{11} parameter of the antenna using the varactor equivalent circuit.

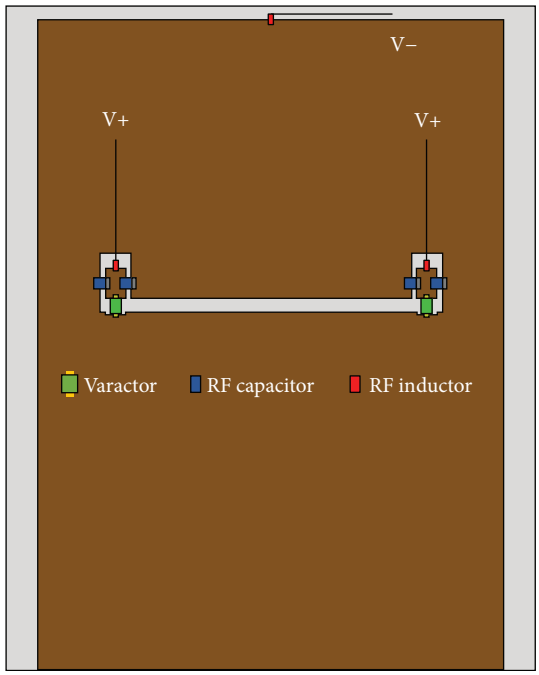

FIGURE 14: Biasing circuit configuration.

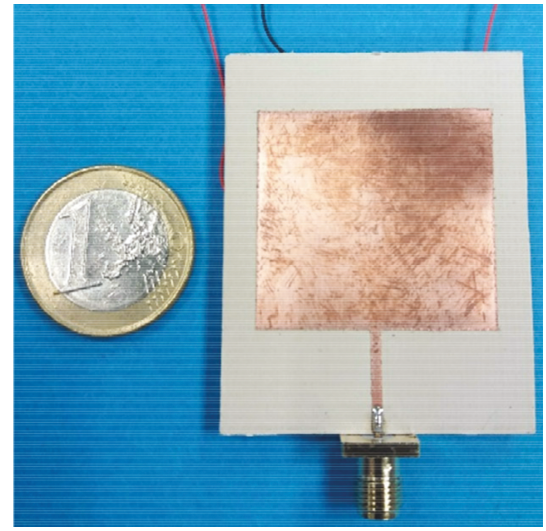

(a)

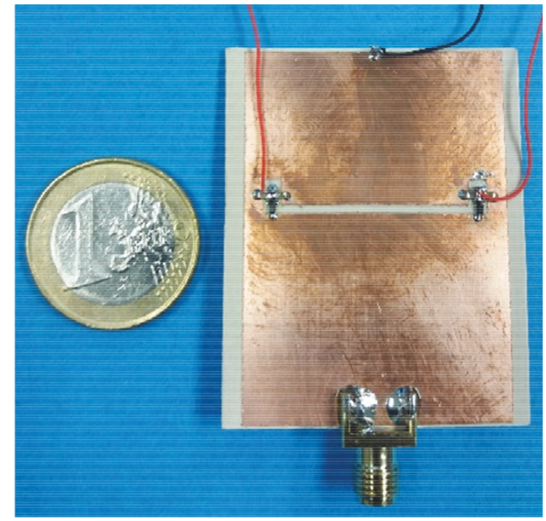

(b)

FIGURE 15: Fabricated antenna with DC bias circuit. (a) Front view. (b) Back view.

To be noted, the second band is a combination of several modes as seen in the previous section, and it is observed that the length and the width of the rectangular patch affect this band. As a suggestion, this band could be tuned as well by following the approach in [17] by embedding a pair of capacitors in the two opposite corners of the rectangular patch.

For the simulation of the structure including varactors, two approaches are followed in order to obtain good simulation performance. The first method consists of using the fundamental lumped element of the varactor diode, which is purely a capacitor. The second manner is based on using the equivalent circuit of the diode varactor given by the manufacturer, which include capacitors, inductance, and resistance.

(1) Case1: Ideal Circuit. Base on the typical capacitance of each voltage in the datasheet of the SMV2025 varactor diode model, a capacitor is used to simulate the diode varactor function. In Figure 10, by altering the capacitance values, the frequency of the first band is shifted reversely to the capacitor value and a smooth variation in a wide frequency range achieved. The second band keeps it constancy while the capacitors are varied. Remark that this simulation approach is called ideal case which did not include any parasitic element.

(2) Case2: Equivalent Circuit. For better simulation performance, this case includes the lumped elements in the equivalent circuit of the varactor. The tuning capacitance C_T ranges from 8.81 pF to 1.15 pF and can be achieved by the means of the reverse bias from 0 V to 20 V. The varactor diode model adopted in this antenna offer very low parasitic inductance and capacitance. Figure 11 shows the equivalent circuit of the varactor diode and antenna

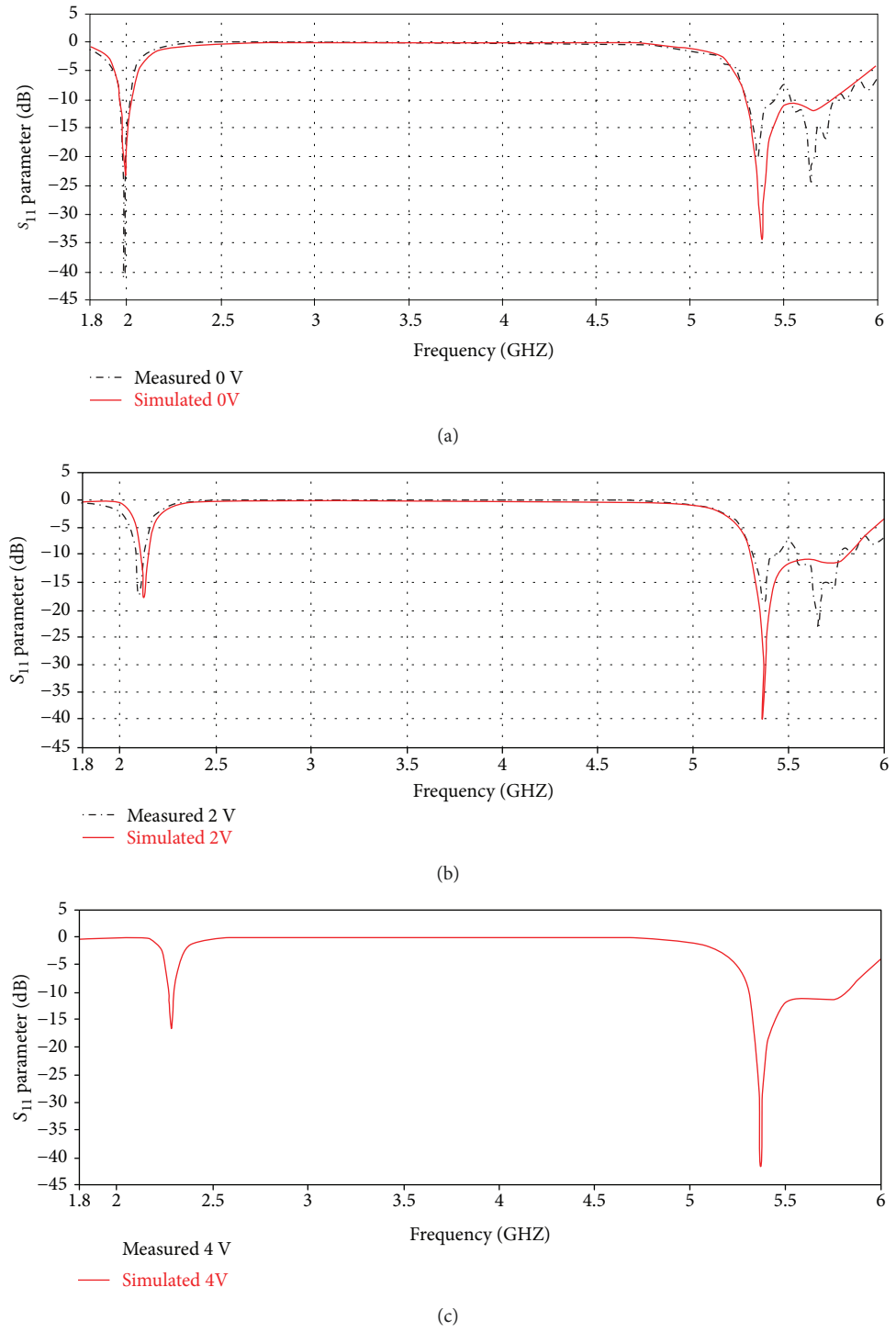

FIGURE 16: Simulated vs. measured S_{11} parameter for different biasing voltages: (a) 0 V, (b) 2 V, and (c) 4 V.

schematic model, where L_S is the parasitic inductance, R_S is the series resistance of the diode, C_T is the variable junction capacitance of the diode, and C_P is the parasitic capacitance arising from the installation of the package material. Figure 12 shows the variation of the frequency according to the capacitor variation. It can be seen that with this varactor model, a wide reconfigurable frequency band is achieved, from 2 GHz to 3.8 GHz.

The S_{11} parameter for both approaches are shown in Figures 10 and 13, showing a good agreement. The first band is a reconfigurable band, while the second is a steady band. A small shift in frequency can be observed in the second case, due to the additional parasitic components added. It can be seen that the impedance matching is below -10 dB for all the bands. The -10 dB bandwidth for the reconfigurable bands varies from 50 to 10 MHz,

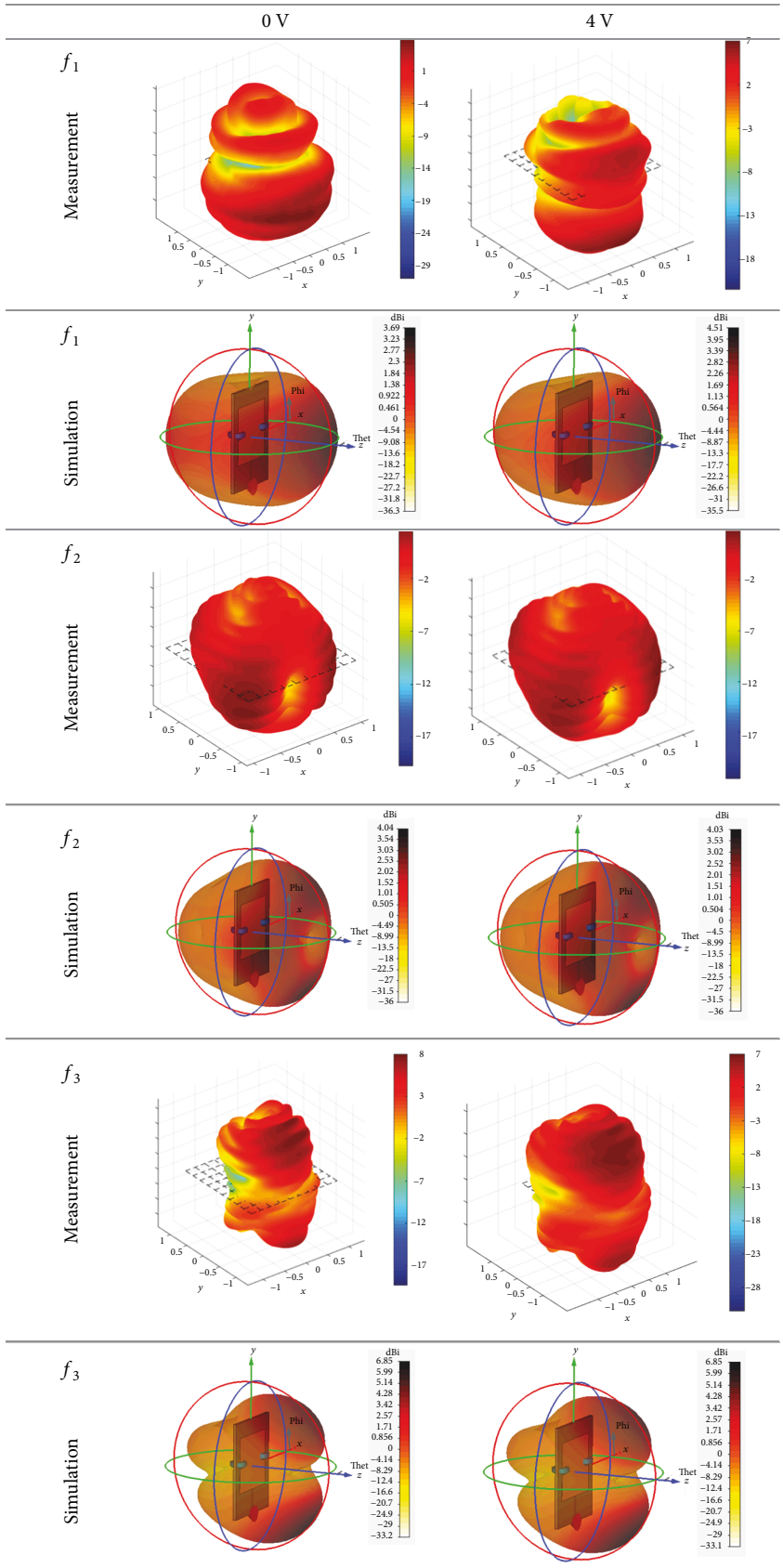

Figure 17: Simulated and measured 3D radiation patterns.

whereas for the steady band the impedance bandwidth reaches 500 MHz.

4. Prototype and Measurement Results

The bias circuit of the varactor diodes is loaded in a suitable manner, and DC components for controlling the varactor diodes are fitted in the ground plane. As illustrated in Figure 14, four DC block capacitors of 40 pF are used, in order to conserve the continuity of the RF current in the ground plane and provide DC blocking. DC voltage is isolated from the RF signal using three RF inductors of 40 nH. The cathode of the varactor diodes is connected to a small copper area and supplied with the positive DC voltage, while the anodes of the varactor diodes are connected to the ground plane, where the negative terminal is connected. The prototype of the antenna as depicted in Figure 15 is tested and analyzed.

Figure 16 illustrates a comparison between simulated and measured S_{11} parameter for three different biasing voltages 0 V, 2 V, and 4 V, as the bias increase, the capacitance decrease and the frequency shifted to the upper bands. It can be seen that at the reconfigurable band (lower band), a good agreement in the first configuration shown in Figure 16(a) (lower band centered at 2 GHz) and second configuration shown in Figure 16(b) (lower band centered at 2.15 GHz) is observed. The corresponding equivalent capacitance to the biasing voltages of 0 V and 2 V is 8.81 pF and 4.67 pF, respectively. The third configuration in Figure 16(c) (lower band centered at 2.25 GHz) does not meet a perfect match between simulation and measurement, due to the unstable behavior of bias circuit as the frequency increases. However, any selectable frequency at 2 GHz band can be achieved slightly by biasing reversely the varactor.

The radiation patterns of the prototype antenna were measured for the two configurations of biasing voltages (0 V and 4 V). The 3D patterns were taken at three selected operating frequencies within the reconfigurable band ($f_1 = 2$ GHz for 0 V and $f_1 = 2.3$ GHz for 4 V and two frequencies (f_2 and f_3) within the steady band ($f_2 = 5.4$ GHz and $f_3 = 5.67$ GHz)).

As shown in Figure 17, the majority of the measured patterns agree well with the simulated ones. Remark that some difference between the simulated and measured patterns for the first configuration (f_1, 0 V) exists, due to slight differences between the simulated and physical feeding adjustments.

Measured efficiency for the antenna in the steady band is above 66%, whereas the efficiency of the reconfigurable bands when the varactor is biased with 0 V and 4 V is 49% and 89%, respectively. These values are acceptable for real applications. In addition, the measured gains of the first and second bands are 3.16 dB and 6.56 dB (when 0 V is applied) and 6.33 dB and 5.67 dB (when 4 V is applied).

5. Conclusions

A practical approach to design dual-band frequency reconfigurable antenna is proposed. Based on the characteristic mode analysis, the ability to tune a particular mode instead of the rest of modes is demonstrated. Two simulation methods have been proposed, ideal case and equivalent circuit case. The interpretation is successfully applied to design a reconfigurable antenna that entirely covers the 2 GHz band and with a steady band centered at 5 GHz. The simulated results using the equivalent circuit of the varactor diode and the measured results are in good agreement.

Data Availability

The results used to support the findings of this study will be supplied under request to the corresponding author.

Conflicts of Interest

The authors declare that they have no conflicts of interest.

Acknowledgments

This work has been supported by the Spanish Ministry of Science, Innovation and Universities (Ministerio Ciencia, Innovación y Universidades) under the project TEC2016-78028-C3-3-P.

References

[1] F. Zhu, S. Gao, A. T. S. Ho et al., "Multiple band-notched UWB antenna with band-rejected elements integrated in the feed line," *IEEE Transactions on Antennas and Propagation*, vol. 61, no. 8, pp. 3952–3960, 2013.

[2] H. M. Al-Tamimi and S. Mahdi, "A study of reconfigurable multiband antenna for wireless application," *International Journal of New Technology and Research*, vol. 2, no. 5, pp. 125–134, 2016.

[3] Z. Mahlaoui, E. Antonino-Daviu, M. Ferrando-Bataller, H. Benchakroun, and A. Latif, "Frequency reconfigurable patch antenna with defected ground structure using varactor diodes," in *2017 11th European Conference on Antennas and Propagation (EUCAP)*, pp. 2217–2220, Paris, France, March 2017.

[4] Y. H. Cui, P. P. Zhang, and R. L. Li, "Broadband quad-polarisation reconfigurable antenna," *Electronics Letters*, vol. 54, no. 21, pp. 1199-1200, 2018.

[5] K. Boonying, C. Phongcharoenpanich, and S. Kosulvit, "Polarization reconfigurable suspended antenna using RF switches and P-I-N diodes," in *The 4th Joint International Conference on Information and Communication Technology, Electronic and Electrical Engineering (JICTEE)*, pp. 1–4, Chiang Rai, Thailand, March 2014.

[6] P. Y. Qin, Y. J. Guo, and C. Ding, "A dual-band polarization reconfigurable antenna for WLAN systems," *IEEE Transactions on Antennas and Propagation*, vol. 61, no. 11, pp. 5706–5713, 2013.

[7] I. T. E. Elfergani, A. S. Hussaini, C. H. See et al., "Printed monopole antenna with tunable band-notched characteristic for use in mobile and ultra-wide band applications," *International Journal of RF and Microwave Computer-Aided Engineering*, vol. 25, no. 5, pp. 403–412, 2015.

[8] N. Nguyen-Trong, L. Hall, and C. Fumeaux, "A frequency and pattern reconfigurable center shorted microstrip antenna,"

IEEE Antennas and Wireless Propagation Letters, vol. 15, pp. 1955–1958, 2016.

[9] M. D. Wright, W. Baron, J. Miller, J. Tuss, D. Zeppettella, and M. Ali, "MEMS reconfigurable broadband patch antenna for conformal applications," *IEEE Transactions on Antennas and Propagation*, vol. 66, no. 6, pp. 2770–2778, 2018.

[10] Q. Liu, N. Wang, C. Wu, G. Wei, and A. B. Smolders, "Frequency reconfigurable antenna controlled by multi-reed switches," *IEEE Antennas and Wireless Propagation Letters*, vol. 14, pp. 927–930, 2015.

[11] R. B. V. B. Simorangkir, Y. Yang, R. M. Hashmi, T. Bjorninen, K. P. Esselle, and L. Ukkonen, "Polydimethylsiloxane-embedded conductive fabric: characterization and application for realization of robust passive and active flexible wearable antennas," *IEEE Access*, vol. 6, pp. 48102–48112, 2018.

[12] D. Guha, S. Biswas, and C. Kumar, "Printed antenna designs using defected ground structures: a review of fundamentals and state-of-the-art developments," *Forum for Electromagnetic Research Methods and Application Technologies*, vol. 2, pp. 1–13, 2014.

[13] E. Antonino-Daviu, M. Cabedo-Fabres, M. Sonkki, N. Mohamed Mohamed-Hicho, and M. Ferrando-Bataller, "Design guidelines for the excitation of characteristic modes in slotted planar structures," *IEEE Transactions on Antennas and Propagation*, vol. 64, no. 12, pp. 5020–5029, 2016.

[14] R. Harrington and J. Mautz, "Theory of characteristic modes for conducting bodies," *IEEE Transactions on Antennas and Propagation*, vol. 19, no. 5, pp. 622–628, 1971.

[15] Skyworks Solution inc, "SMV2025 series: surface mount, silicon hyperabrupt tuning varactor diodes," *SMV2025 Series Data sheet*, 2015, http://www.skyworksinc.com/uploads/documents/SMV2025_Series_201431E.pdf.

[16] C. A. Balanis, *Antenna Theory: Analysis and Design*, Wiley, Hoboken, NJ, USA, 3rd edition, 2005.

[17] I. Rouissi, I. B. Trad, J.-M. Floc'h, H. Rmili, and H. Trabelsi, "Design of frequency reconfigurable triband antenna using capacitive loading for wireless communications," in *2015 Loughborough Antennas & Propagation Conference (LAPC)*, Loughborough, UK, November 2015.